Materials Research Proceedings 28 (2023) 321-330 https://doi.org/10.21741/9781644902479-35

Gate design algorithm to maximize the fiber orientation effectiveness in thermoplastic injection-molded components

PERIN Mattia[1,a], BERTI Guido A.[1,b], LEE Taeyong[2,3,c] and QUAGLIATO Luca[2,3,d *]

[1]Department of Management and Engineering, University of Padua, 36100, Vicenza, Italy

[2]Division of Mechanical and Biomedical Engineering, Ewha Womans University, Seoul 03760, Republic of Korea

[3]Division of Mechanical and Biomedical Engineering, Graduate Program in System Health Science and Engineering, Ewha Womans University, Seoul 03760, Republic of Korea

[a] mattia.perin@phd.unipd.it, [b] guido.berti@unipd.it, [c] tlee@ewha.ac.kr, [d] lucaq@ewha.ac.kr

Keywords: Injection Molding, Fibers Reinforced Composite (FRC), Injection Gate Location, Fiber Orientation, Machine Learning

Abstract. This research presents an automatic algorithm, implemented in a Visual Basic Architecture (VBA), for the optimization of the gate location in thermoplastic injection molding of short fibers reinforced composite materials. The algorithm receives, as input, the geometry of the component and, according to the user's choice, defines the injection points grid, and relevant versors, on a pre-constructed mesh, automatically runs the finite volume method (FVM) simulation and exports the fiber orientation tensor (FOT) on each node of the mesh. The nodal coordinate of the part and the relevant FOT are then used as the training dataset for a Gradient Boosting (GB) algorithm for the full correlation between injection gate locations and the resulting fiber orientation distribution (FOD), allowing to define the injection gate configuration better suited to maximize the effectiveness of the reinforcement fibers. By coupling the trained GB algorithm with a finite element method (FEM) simulation it was confirmed that the developed algorithm can predict the influence of the gate location on the FOD and the resulting mechanical performances, improving the stiffness between 3.8% and 32.6%, on simple and complex geometries alike.

Introduction

In recent years, the injection molding process has been growing in both importance and utilization thanks to the development of innovative polymers and reinforcements [1, 2]. This is especially the case in the automotive industry, where lightweight design [3] and recyclability [4] are becoming ever-growing focus points for research and development. Although injection molding is considered a fairly well-established manufacturing process, several independent parameters must be properly set to achieve a high quality of the molded parts, especially in terms of minimizing warpage, shrinkage, and weld-lines on the critical region of the component [5-7]. Besides, the recent trend is to incorporate woven composite into an injection-molded thermoplastic matrix to achieve recyclability while enhancing the mechanical properties of the molded part [8].

For the case of short fibers-reinforced thermoplastic polymers (SFRTP) the fiber orientation is influenced by both the component geometry and the injection gates configuration. As it is well known from various recent contributions, fiber orientation is responsible for static, fatigue, and fracture properties of SFRTP [9, 10]. In addition, as demonstrated for both short glass fibers (SGF) and short carbon fibers (SCF), the interaction between polymer matrix and fibers reinforcement plays a pivotal role in controlling the notch sensitivity [11, 12]. Accordingly, controlling and optimizing the fiber orientation in injection molded components becomes of paramount importance to maximize the effectiveness of the reinforcement.

For SFRTP, the fiber orientation distribution (FOD) is influenced by both the injection gates and the geometry of the component, and in a lesser manner by the applied processing conditions. The component geometry varies from case to case and is not easy to generalize. For this reason, recent contributions dealing with the optimization of injection-molded components focused on controlling the global thickness distribution and inserting local rib networks to limit the warpage [13, 14]. On the other hand, injection gate (IG) design has also attracted the interest of researchers over the years, and various modeling technics have been applied to achieve greater optimization considering different criteria, as hereafter summarized.

Zhai et al. [15, 16] developed a recursive approach and a sequential linear programming algorithm to identify the IG locations, allowing for a balanced filling on injection-molded parts. The optimization criterion is based on a uniform distribution of the clamping force during the filling phase and was validated on a U-shape part. Li et al. [17] developed a black-box algorithm for the optimization of the IG considering the injection pressure, warpage, residual stress, and weld lines as optimization criteria. Similarly, Moayyedian and Mamedov [18] proposed a multi-objective optimization approach to defining the combination of process parameters and IG locations, allowing for a reduction of the molding defects, such as shrinkage, warpage, and short shot. More recently, Moayyedian and Mamedov [19] also proposed a methodology for the reduction of the same molding defects but based on an artificial neural network and Taguchi techniques, showing a relatively low margin error, quantified in 15%, and attributed to uncontrollable process variability. Besides, the only contribution dealing with fiber orientation optimization for the SFRTP focuses on the IM process parameters, thus the IG location was considered a constant in the analysis [20]. Other recent contributions proposed case studies investigating the effect of different IG configurations, and process parameters, on the filling time and quality of the molded component [21-23]. However, being these highly customized approaches, they can hardly be extended to different geometries and, most of all, they are all based on unfilled thermoplastic polymers. Accordingly, a general and customizable design approach for the gate location in the case of SFRTP seems to be missing in the literature,

To this aim, this research presents an algorithm able to automatically set up a user-defined number of injection molding FVM simulations, implemented in Autodesk Moldflow Insight 2023, run them, and export the fiber orientation tensor (FOT) on one or more control volumes defined by the user. The coordinates IG points, relevant versors, and the average fiber orientation tensor in the control volumes of interest are used to train and validate a machine learning (ML) model, based on the Gradient Boosting (GB) algorithm.

The proposed algorithm can suggest the best IG location allowing for the maximization of the FOD along one or more regions of interests and directions, with assigned priorities, resulting in customized stiffness enhancement. The maximization is carried out considering the load path, thus the directions along which the reaction forces are maximum, because of the applied displacements. The procedure has been developed and tested considering three geometries with an increasing level of feature complexity by mapping the FOD and relevant mechanical properties from the FVM simulation onto the FEM simulation, implemented in Abaqus 2020. The application of the IG optimization procedure allowed improving the component's stiffness between 3.8% and 32.6%, showing the effectiveness and the generality of the proposed algorithm.

Materials and Methods

This chapter is subdivided into three sections. The first deals with the proposed VBA algorithm for the automatic definition of the injection gate grid and the export of the FOD from each one of the FVM simulations. The first section also includes some details of the implemented machine learning model, based on the Gradient Boosting (GB) algorithm. The second section briefly describes the material properties of the employed polyamide-6 reinforced with 20% of short carbon fibers (PA6-20CF) and the relevant calibration into the FVM simulation. Finally, the third section

explains the mapping procedure for the transfer of the FOD, and relevant mechanical properties, from the FVM to the FEM simulation, for the evaluation of the stress distribution on the considered components as a consequence of the applied displacements.

Gate Location Optimization Algorithm

The IG location optimization algorithm is composed of four steps, as summarized in Fig. 1. All the steps are implemented in VBA programming, except for the ML-GB model of step#4, implemented in Python 3.11 and coupled with the scikit-learn 1.1.1 and SciPy 1.7.1 open-source libraries. In the algorithm, step#1 is devoted to the definition of the IG candidates on the selected model geometry that can be defined by the user on a predetermined grid or manually deployed. Step#2 receives the matrix with the IG candidates, and their relevant versors, to assure a perpendicularity onto the geometry and prepares the input files for the FVM simulation, comprehensive of all IG configurations to be tested.

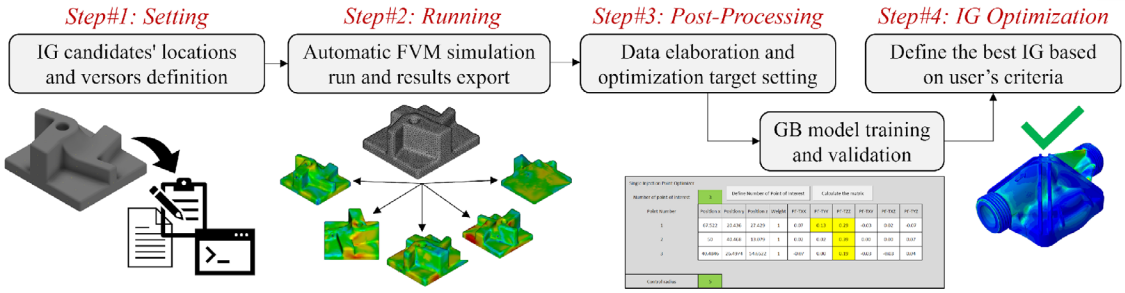

Fig. 1. Working flow for the injection gate (IG) optimization algorithm.

After the completion of all FVM simulations setup in step#2, step#3 creates a single result dataset file including i) coordinates of the IG point, ii) coordinates of all the nodes of the mesh (same for each simulation), and iii) results of the FOT (6 components) for each node. During step#3, the user is required to input the locations of interest and the relevant direction, or directions, along which the FOD should be oriented. To this aim, FEM simulations have been utilized to identify the regions of interest on the considered parts and, within those regions, the directions along which the stress components are maximum. Thus, by aligning the fibers along these directions, their effectiveness can be improved, allowing for an improvement in stiffness.

Before reaching step#4, the dataset constructed in step#3 is utilized to train and validate the prediction part of the architecture, based on the GB algorithm. 80% of the database is utilized for training purposes, whereas the remaining 20% is dedicated to validation. During the training, a k-fold validation, with k=5, is employed to assure accuracy and the absence of overfitting. If both conditions are satisfied, the user is presented with the location of the IG allowing for the maximization of the FOD in the locations of interest.

At this point, two important clarifications must be made. First, if the user is not satisfied with the accuracy of the prediction carried out by the GB model, the procedure can be upgraded by setting a finer grid for the IG location candidates in step#1, where only the new FVM simulations must be run and then integrated with those of the previous phase. Second, the proposed methodology considers only a single injection gate. Future studies are going to be focused on the direction of multiple IG optimization for better applicability in industrial applications.

Material Properties and FVM Simulation Setting

For the setting of the FVM simulations, the material properties relevant for the PA6-20CF material, as calibrated in previous works of one of the authors [9, 10, 12], have been employed. For their calibration into the FVM simulation, necessary for the subsequent mapping onto the FEM mesh,

the Ramberg-Osgood constitutive model, Eq. 1, has been employed and coupled with an anisotropic Hill'48 yield function, Eq. 2. The α and β parameters are calculated according to the FOT, for each element of the mesh as in Eq. 3, referring to the region of the model where it is maximum. In Eq. 3, λ_I represents the first eigenvalue of the fiber orientation tensor on each element of the mesh, whereas α_m, β_m and $\lambda_{m,I}$, are the reference values for the considered material, and are calculated during the material properties calibration. Fig. 2 shows the experimental engineering stress-strain curves for the considered PA6-20CF material (Fig. 2a), the comparison between experimental and constitutive modeling load-displacement curves (Fig. 2b), and model constants and reference values for the Ramberg-Osgood and anisotropic Hill'48 models (Fig. 2c).

$$\sigma = E^{1/n}\left(K\right)^{(n-1)/n}\left(\varepsilon_{p,eff}\right)^{1/n} \tag{1}$$

$$\sigma_{eff} = \sqrt{\frac{\left(\alpha\sigma_{11}-\beta\sigma_{22}\right)^2+\left(\beta\sigma_{22}-\beta\sigma_{33}\right)^2+\left(\beta\sigma_{33}-\alpha\sigma_{11}\right)^2+6\left[\left(\sigma_{12}\right)^2+\left(\sigma_{23}\right)^2+\left(\sigma_{31}\right)^2\right]}{2}} \tag{2}$$

$$\alpha\left(\lambda_I\right)=\theta+\left[\frac{\left(\alpha_m-\theta\right)}{\left(\lambda_{m,I}-1/2\right)}\right]\left(\lambda_I-1/2\right) \quad , \quad \beta\left(\lambda_I\right)=\theta+\left[\frac{\left(\beta_m-\theta\right)}{\left(\lambda_{m,I}-1/2\right)}\right]\left(\lambda_I-1/2\right) \tag{3}$$

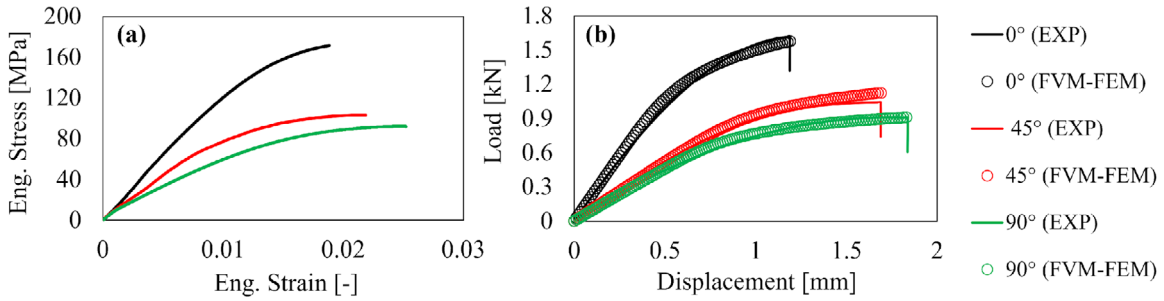

(c)

Parameter	Definition	Value
K	Strength coefficient	80.6 MPa
n	Hardening exponent	10.16
E_m	Polymer matrix elastic modulus	4.25 GPa
E_f	Fiber elastic modulus	105.6 GPa

Parameter	Definition	Value
α_m	Weight factor for the fiber direction	2.125
β_m	Weight factor for the direction normal to the fibers	1.214
$\lambda_{m,I}$	First eigenvalue of the fiber orientation matrix (strong fibers alignment region)	0.85

Fig. 2. (a) Materials properties and (b) comparison between experimental and constitutive modeling results of load-displacement curves for 0°, 45°, and 90° directions. (c) Model constants for the Ramberg-Osgood model and anisotropic Hill'48 yield function.

As concerns the mesh for the FVM simulation, the same mesh strategy, 3mm side 3D tetrahedral elements, has been employed and verified through mesh sensitivity analysis. In terms of injection molding process parameters, to avoid any bias, the same mold temperature, molten material temperature (at the nozzle), and cooling temperature of 285°C, 85°C, and 25°C, have been employed in all simulations. Regarding the injection time, it has been kept automatically controlled during the simulation, to avoid short-shot, whereas the post-pressure has been set at 80% of the injection pressure, for a total of 20s.

FVM-FEM Mapping and Tested Components

To test the improvement of the FOD with respect to the applied displacements, a mapping procedure to account for the FOD-dependent material properties in the structural FEM simulation has been employed. The structural FEM simulation has been implemented in ABAQUS 2020. The procedure is summarized in Fig. 3 and is based on the Ramberg-Osgood and anisotropic Hill'48 formulations presented in the previous section whereas the mapping is carried out by Autodesk Helius 2023.

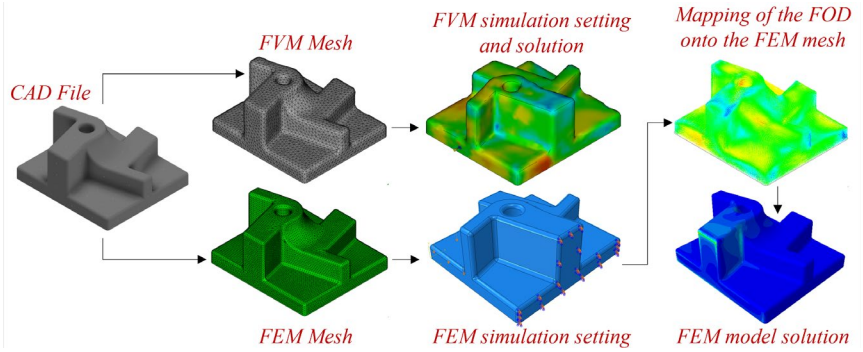

Fig. 3. Main steps in the mapping procedure for the consideration of the fiber orientation of the FVM simulation into a FEM structural simulation environment.

For each element of the FVM mesh, a corresponding set of elements in the FEM mesh is located based on their relevant position in the GCS, the same for both simulations. According to the FOT of each element of the FVM simulation, a specific set of mechanical properties is mapped onto the FEM simulation mesh. This procedure has been successfully applied and validated in other works of one of the corresponding author [9, 10, 12]. To test the IG design algorithm, three components have been considered, as shown in Fig. 4. The three parts have an increasing level of complexity and have all been subjected to a tensile displacement of 5 mm.

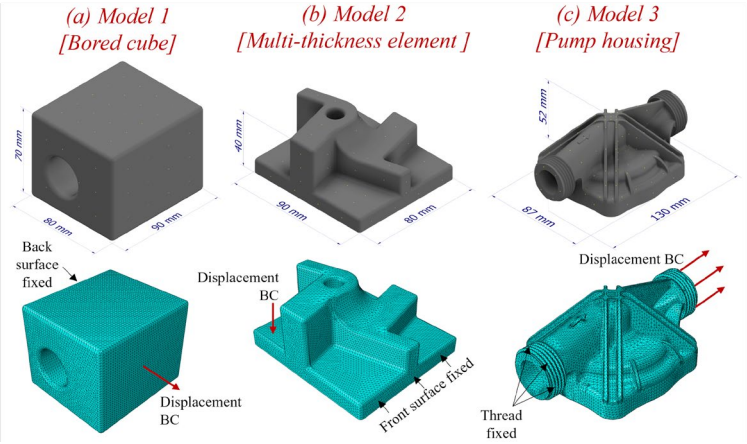

Fig. 4. Mechanical parts use for the validation of the IG location design algorithm. (a) Bored cube, (b) Multi-thickness element on a square base, and (c) Pump housing.

The three geometries of Fig. 4 have been all meshed with C3D10I tetrahedron elements, thanks to their good compatibility with those of the FVM simulation, whereas a quadratic integration scheme has been employed to allow for a better description of the deformation behavior between the edges and within the elements. The total number of elements for the three models is 306,165 (Fig. 4a), 243,183 (Fig. 4b), and 211,149 (Fig. 4c), respectively. The FEM simulations have been implemented in the ABAQUS/Standard environment, considering a static-implicit solution

technique. Finally, the simulation time has been divided into 100 steps for easier export and comparison of the results among the simulation cases of the same part.

Results and Discussion

To validate the IG location optimization algorithm, the procedure summarized in Fig. 1 has been applied to the three components of Fig. 4. The results, and relevant considerations, are reported in this chapter of the paper.

The initial step, prior to the application of the IG design algorithm, is the identification of the regions of the model subjected to high stress, or stress concentration, due to the displacement boundary conditions, or specific geometrical features. Accordingly, three FEM simulations considering only elastic material properties equal to E = 14GPa and ν = 0.37, representative of a sort of 0° direction for the PA6-20CF material, have been implemented. The results, reported in Fig. 5, allowed identifying two regions of interest for Model 1, four for Model 2, and three for Model 3, respectively. In Fig. 5, the normalized stress components (-1, +1 range) on the regions of interest are reported and are utilized as a reference for the directions along which to maximize the FOD. Rather than a quantitative estimation, the aim of this preliminary phase is the definition of the regions of the model where to focus on the optimization of the effectiveness of the FOD.

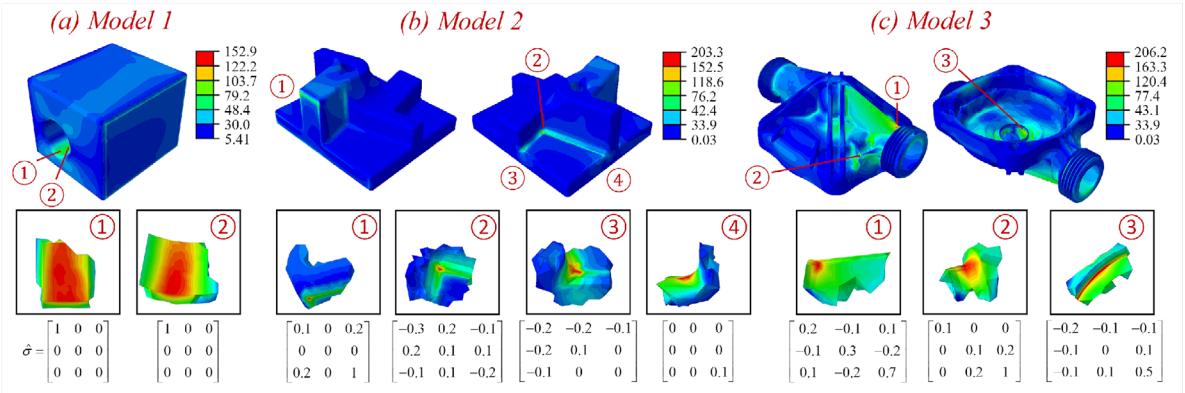

Fig. 5. Identification of the regions of interest from isotropic properties FEM for (a) Bored cube, (b) Multi-thickness element on square base, and (c) Pump housing models.

As defined in Fig. 1, the algorithm requires the definition of a mesh grid and the list of the IG candidates, with relevant versors, to assure perpendicularity with the geometry. For the three models of Fig. 4, 80, 70, and 140 IG candidate locations have been randomly assigned on an automatically generated 3 mm mesh grid in the relevant FVM simulations. The results, in terms of stress components ($\sigma_{x,y,z}$) for the best and worst IG locations, among the tested candidates, for the three tested components, are reported in Fig. 6a, 6b, and 6c, respectively.

The stress components of Fig. 6 are the average values relevant to a control volume of R = 5 mm around the element with the peak stress. As expected, a lower fibers alignment along the directions of loading (load path) results in a lower stress component along the same direction, a fact caused by a lower stiffness of the material. Since all simulations have been set up considering a displacement boundary condition, the reaction force is calculated according to the material properties, Fig. 2a. Thus, the higher the alignment of FOD with the reaction force direction, caused by the applied displacement boundary condition [9, 10], the higher the resulting stress.

This fact is clear when analyzing the difference between the best and worst IG configurations, for all three components reported in Fig. 6. For instance, in Model 1, due to the proximity of the two regions of interest, the average improvement is around +30%. For more complex parts, such as Model 2, the improvement is represented by a reduction of the compressive stresses, which has also a positive effect on the performances of the component due to the low compressive strength

of fibers reinforced materials. In general, the IG design algorithm gives priority to the regions identified by a high normalized value, as shown in Fig. 5. On the other hand, in some conditions, the optimization may result in a higher improvement of the effectiveness of the reinforcement in a region of the model which is not the main priority. This is clearly visible from the results of Fig. 6c, where region ③ shows a higher stiffness improvement than region ②, although the latter has the highest priority according to the normalized stress presented in Fig. 5c.

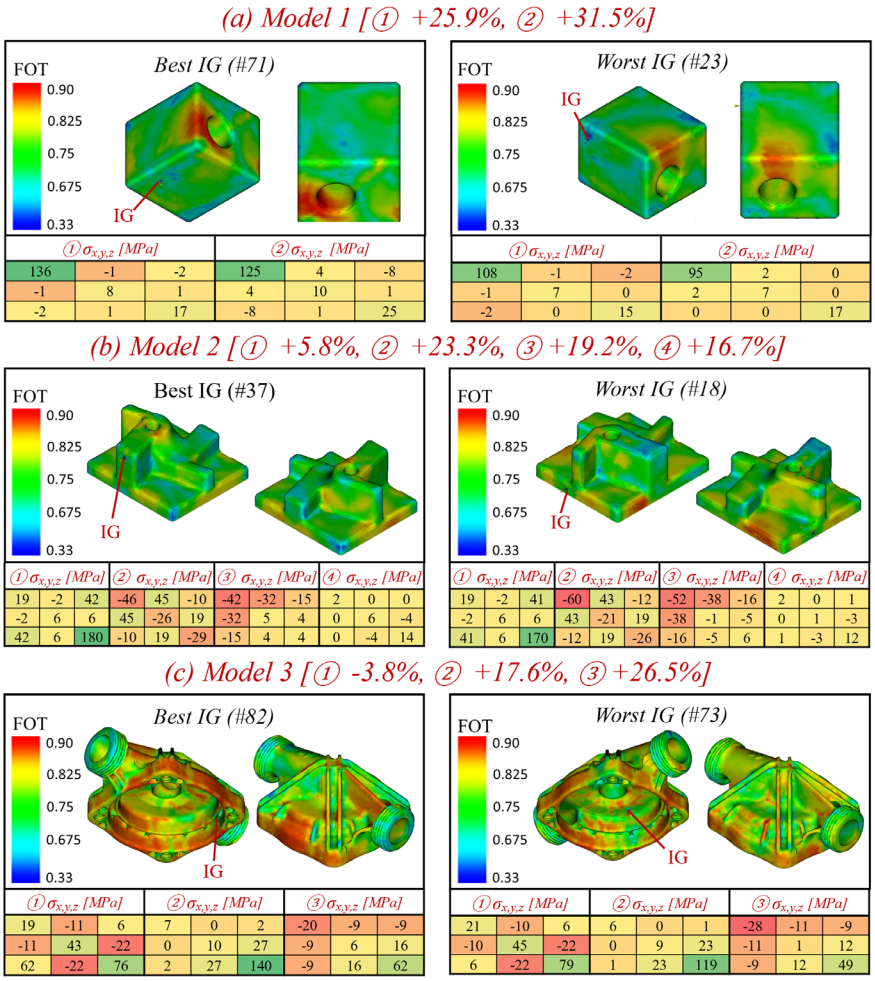

Fig. 6. FOT distribution (FVM simulation) and stress components (FEM simulation) for the best and worst IG locations for (a) Model 1, (b) Model 2, and (c) Model 3.

From a general perspective, it is interesting to highlight that, according to the results presented in Fig. 6, for all three models and even before the final optimization stage, implemented through the ML-GB algorithm, the average improvement in terms of FOD is clear and quantified in 28.7%, 16.3%, and 13.4% for the three investigated components. The almost two times higher stiffness improvement estimated for the bored cube part is related to the relative simplicity of the geometry, which makes it easier for the IG optimization algorithm to identify the best IG location.

In order to achieve full optimization for the IG location, the FOD resulting from the FVM simulations of each of the three components have been utilized for training and validation for the ML-GB algorithm. The average deviations between true and predicted values for the FOD for the components have been calculated at 5.6%, 4.8%, and 3.5% for the training datasets, and 5.2%,

4.8%, and 3.4%, for the validation datasets, respectively. These deviations are the average ones relevant for the 5-fold validations and show the quality of the prediction and the absence of bias.

By employing the trained GB model, further improvements on the FOD could be achieved, as reported in Fig. 7. For the case of Model 1, due to the low complexity of the geometry, the FVM simulation-based analysis was sufficient in identifying a fairly good IG location, thus the stiffness improvement provided by the application of the GB algorithm is minimal. However, for both Model 2 and Model 3, the application of the trained GB model allowed identifying a better IG location, not previously included in the FVM simulation database, which achieved a further improvement of the effectiveness of the fibers reinforcement. For Model 2 the average stiffness improvement, with respect to the results of Fig. 6, is quantified in 4.6%, whereas for Model 3 is it quantified in 3.3%.

(a) Model 1 [① +2.2%, ② +0.8%]

After Gradient Boosting Optimization					
① $\sigma_{x,y,z}$ [MPa]			② $\sigma_{x,y,z}$ [MPa]		
139	-2	2	126	2	0
-2	9	1	2	10	1
2	1	15	0	1	20
Before Gradient Boosting Optimization					
136	-1	-2	125	4	-8
-1	8	1	4	10	1
-2	1	17	-8	1	25

(c) Model 3 [① +7.9%, ② +2.1%, ③ +0%]

After Gradient Boosting Optimization								
① $\sigma_{x,y,z}$ [MPa]			② $\sigma_{x,y,z}$ [MPa]			③ $\sigma_{x,y,z}$ [MPa]		
21	-12	7	7	0	2	-19	-10	-11
-12	46	-24	0	10	27	-10	5	15
7	-24	82	2	27	143	-11	15	62
Before Gradient Boosting Optimization								
19	-11	6	7	0	2	-20	-9	-9
-11	43	-22	0	10	27	-9	6	16
62	-22	76	2	27	140	-9	16	62

(b) Model 2 [① +5%, ② +8.7%, ③ +4.8%, ④ +0%]

After Gradient Boosting Optimization											
① $\sigma_{x,y,z}$ [MPa]			② $\sigma_{x,y,z}$ [MPa]			③ $\sigma_{x,y,z}$ [MPa]			④ $\sigma_{x,y,z}$ [MPa]		
22	-2	43	-42	43	-11	-40	-37	-15	2	0	1
-2	4	1	43	-24	22	-37	1	-4	0	6	-4
43	1	189	-11	22	-34	-15	-4	6	1	-4	14
BeforeGradient Boosting Optimization											
19	-2	42	-46	45	-10	-42	-32	-15	2	0	0
-2	6	6	45	-26	19	-32	5	4	0	6	-4
42	6	180	-10	19	-29	-15	4	4	0	-4	14

Fig. 7. Stress components for the best IG locations before and after the GB-IG optimization for (a) Model 1, (b) Model 2, and (c) Model 3

Summary

The research presented in this paper detailed a highly customizable algorithm for the optimization of the injection gate location in the thermoplastic injection molding process for the maximization of the effectiveness of the fibers reinforcement in SFRC. The IG prediction algorithm proved to be able to achieve a concurrent optimization of the FOD in various regions of interest while prioritizing those with the highest stress distribution. Being implemented on freeware SW, the proposed algorithm can be implemented directly to various components, from low to high complexity, allowing for higher exploitation of the potentials of SFRC. On the other hand, as also previously mentioned, more research work should be oriented on extending the proposed methodology to multi-gate injection molding, to allow for the application to bigger geometries where a single IG is not sufficient. In addition to that, the influence of the injection molding process parameters on the FOD is going to be accounted for as well, to allow for a more comprehensive and realistic prediction and optimization of the IG locations.

Acknowledgments

This research was supported by the BK21 FOUR (Fostering Outstanding Universities for Research) funded by the Ministry of Education (MOE, Korea) and National Research Foundation of Korea (NRF-5199990614253).

References

[1] T. Ishikawa, K. Amaoka, Y. Masubuchi, T. Yamamoto, A. Yamanaka, M. Arai, J. Takahashi, Overview of automotive structural composites technology developments in Japan, Compos. Sci. Technol. 155 (2018) 221-246. http://doi.org/10.1016/j.compscitech.2017.09.015

[2] P. Boisse, R. Akkerman, P. Carlone, L. Kärger, S.V. Lomov, J.A. Sherwood, Advances in composite forming through 25 years of ESAFORM, Int. J. Mater. Forming 15 (2022) 39. https://doi.org/10.1007/s12289-022-01682-8

[3] L. Quagliato, C. Jang, N. Kim, Manufacturing process and mechanical properties characterization for steel skin – Carbon fiber reinforced polymer core laminate structures, Compos. Struct. 209 (2019) 1-12. http://doi.org/10.1016/j.compstruct.2018.10.078

[4] T. Evens, G.-J. Bex, M. Yigit, J. De Keyzer, F. Desplentere, A. Van Bael, The influence of mechanical recycling on properties in injection molding of fiber-reinforced polypropylene, Int. Polym. Process. 34 (2019) 398-407. http://doi.org/10.3139/217.3770

[5] N.Y. Zhao, J.Y. Lian, P.F. Wang, Z.B. Xu, Recent progress in minimizing the warpage and shrinkage deformations by the optimization of process parameters in plastic injection molding: a review, Int. J. Adv. Manuf. Technol. 120 (2022) 85-101. http://doi.org/10.1007/s00170-022-08859-0

[6] S. Kitayama, S. Hashimoto, M. Takano, Y. Yamazaki, Y. Kubo, S. Aiba, Multi-objective optimization for minimizing weldline and cycle time using variable injection velocity and variable pressure profile in plastic injection molding, Int. J. Adv. Manuf. Technol. 107 (2020) 3351-3361. http://doi.org/10.1007/s00170-020-05235-8

[7] E.I. Kurkin, O.E. Lukyanov, V.O. Chertykovtseva, O.U. Espinosa Barcenas, Molding gate optimization for weld line location away from structures loaded area, J. Phys.: Conference Series 1925 (2021) 012056. http://doi.org/10.1088/1742-6596/1925/1/012056

[8] E. Jeong, Y. Kim, S. Hong, K. Yoon, S. Lee, Innovative Injection Molding Process for the Fabrication of Woven Fabric Reinforced Thermoplastic Composites, Polym. 14 (2022). http://doi.org/10.3390/polym14081577

[9] L. Quagliato, Y. Kim, J.H. Fonseca, D. Han, S. Yun, H. Lee, N. Park, H. Lee, N. Kim, The influence of fiber orientation and geometry-induced strain concentration on the fatigue life of short carbon fibers reinforced polyamide-6, Mater. Des. 190 (2020) 108569. http://doi.org/10.1016/j.matdes.2020.108569

[10] L. Quagliato, J. Lee, J.H. Fonseca, D. Han, H. Lee, N. Kim, Influences of stress triaxiality and local fiber orientation on the failure strain for injection-molded carbon fiber reinforced polyamide-6, Eng. Fract. Mech. 250 (2021) 107784. http://doi.org/10.1016/j.engfracmech.2021.107784

[11] M. Ricotta, M. Sorgato, M. Zappalorto, Tensile and compressive quasi-static behaviour of 40% short glass fibre - PPS reinforced composites with and without geometrical variations, Theor. Appl. Fract. Mec. 114 (2021) 102990. http://doi.org/10.1016/j.tafmec.2021.102990

[12] L. Quagliato, M. Ricotta, M. Zappalorto, S.C. Ryu, N. Kim, Notch effect in 20% short carbon fibre-PA reinforced composites under quasi-static tensile loads, Theor. Appl. Fract. Mec. 122 (2022) 103649. http://doi.org/10.1016/j.tafmec.2022.103649

[13] J.H. Fonseca, G. Han, L. Quagliato, Y. Kim, J. Choi, T. Keum, S. Kim, D.S. Han, N. Kim, H. Lee, Design and numerical evaluation of recycled-carbon-fiber-reinforced polymer/metal hybrid engine cradle concepts, Int. J. Mech. Sci. 163 (2019) 105115. http://doi.org/10.1016/j.ijmecsci.2019.105115

[14] J.H. Fonseca, L. Quagliato, S. Yun, D. Han, N. Kim, H. Lee, Preliminary design of an injection-molded recycled-carbon fiber–reinforced plastic/metal hybrid automotive structure via

combined optimization techniques, Struct. Multidiscip. O. 64 (2021) 2773-2788. http://doi.org/10.1007/s00158-021-02988-y
[15] M. Zhai, Y. Lam, C. Au, Gate location optimization scheme for plastic injection molding, e-Polymers 9 (2009). https://doi.org/10.1515/epoly.2009.9.1.1515
[16] M. Zhai, Y. Xie, A study of gate location optimization of plastic injection molding using sequential linear programming, Int. J. Adv. Manuf. Technol. 49 (2009) 97-103. http://doi.org/10.1007/s00170-009-2376-1
[17] Z. Li, X. Wang, A Black Box Method for Gate Location Optimization in Plastic Injection Molding, Adv. Polym. Technol. 32 (2013) 793-808. http://doi.org/10.1002/adv.21322
[18] M. Moayyedian, A. Mamedov, Multi-objective optimization of injection molding process for determination of feasible moldability index, Procedia CIRP 84 (2019) 769-773. https://doi.org/10.1016/j.procir.2019.04.213
[19] M. Moayyedian, A. Dinc, A. Mamedov, Optimization of Injection-Molding Process for Thin-Walled Polypropylene Part Using Artificial Neural Network and Taguchi Techniques, Polym. 13 (2021) 4158. https://doi.org/10.3390/polym13234158
[20] K. Li, S.-L. Yan, W.-F. Pan, G. Zhao, Optimization of fiber-orientation distribution in fiber-reinforced composite injection molding by Taguchi, back propagation neural network, and genetic algorithm–particle swarm optimization, Adv. Mech. Eng. 9 (2017) 168781401771922. http://doi.org/10.1177/1687814017719221
[21] M. Huszar, F. Belblidia, H.M. Davies, C. Arnold, D. Bould, J. Sienz, Sustainable injection moulding: The impact of materials selection and gate location on part warpage and injection pressure, Sustainable Mater. Technol. 5 (2015) 1-8. http://doi.org/10.1016/j.susmat.2015.07.001
[22] M.S. Shreyas, L.G. Sannamani, Optimum Gate Location in Injection Mold of Nasal Foreign Body Removal Cover, Int. J. Eng. Res. Technol. 9 (2020) 1-5. http://doi.org/10.17577/IJERTV9IS050010
[23] K. Yang, L. Tang, P. Wu, H. Yi, Research on Optimization of Injection Molding Process Parameters of Automobile Plastic Front-End Frame, Adv. Mater. Sci. Eng. 2022 (2022) 1-18. http://doi.org/10.1155/2022/5955725